1-1-2008

Study on Generalized Analysis Model for Fringe Pattern Profilometry

Y. Hu
University of Wollongong, yingsong@uow.edu.au

Jiangtao Xi
University of Wollongong, jiangtao@uow.edu.au

Z. Yang
Huazhong University of Science and Technology, China

Enbang Li
Univeristy of Wollongong, enbang@uow.edu.au

Joe F. Chicharo
University of Wollongong, chicharo@uow.edu.au

Study on Generalized Analysis Model for Fringe Pattern Profilometry

Abstract

This paper presents a generalized analysis model for fringe pattern profilometry. We mathematically derived a new analysis model that gives a more general expression of the relationship between projected and deformed fringe patterns. Meanwhile, based on the proposed generalized model, a new algorithm is presented to retrieve 3-D surfaces from nonlinearly distorted fringes.Without any prior knowledge about the projection system, we still can obtain very accurate measurement results by using a generalized analysis model and a proposed algorithm. Computer simulation and experimental results show that the generalized model and the proposed algorithm can significantly improve the 3-D reconstruction precision, especially when the projected fringe pattern is nonlinearly distorted.

Disciplines

Physical Sciences and Mathematics

Publication Details

This article was originally published as Hu, Y, Xi, J, Yang, Z, Li, E and Chicharo, JF, Study on Generalized Analysis Model for Fringe Pattern Profilometry, IEEE Transactions on Instrumentation and Measurement, 57(1), 2008, 160-167.

Study on Generalized Analysis Model for Fringe Pattern Profilometry

Yingsong Hu, Jiangtao Xi, *Senior Member, IEEE*, Zongkai Yang, *Senior Member, IEEE*, Enbang Li, and Joe F. Chicharo, *Senior Member, IEEE*

***Abstract*—This paper presents a generalized analysis model for fringe pattern profilometry. We mathematically derived a new analysis model that gives a more general expression of the relationship between projected and deformed fringe patterns. Meanwhile, based on the proposed generalized model, a new algorithm is presented to retrieve 3-D surfaces from nonlinearly distorted fringes. Without any prior knowledge about the projection system, we still can obtain very accurate measurement results by using a generalized analysis model and a proposed algorithm. Computer simulation and experimental results show that the generalized model and the proposed algorithm can significantly improve the 3-D reconstruction precision, especially when the projected fringe pattern is nonlinearly distorted.**

***Index Terms*—Fourier transform profilometry (FTP), fringe pattern analysis, fringe pattern profilometry (FPP), generalized analysis model, shift estimation (SE).**

I. Introduction

FRINGE pattern profilometry (FPP) has been one of the most popular noncontact methods for measuring the 3-D object surfaces in recent years. With FPP, a Ronchi grating or sinusoidal grating is used to project fringe patterns onto a 3-D diffuse surface that results in deformed fringe patterns. The images of the deformed fringe pattern and the original fringe pattern projected on a reference plane are captured by a charge-coupled device (CCD) camera and are processed to reconstruct the profile of objects. To reconstruct the 3-D surface information from the fringe pattern images, a number of fringe pattern analysis methods have been developed, including Fourier transform profilometry (FTP) [1]–[4], phase shifting profilometry [5]–[8], spatial phase detection [9], phase-locked loop profilometry [10], and other analysis methods [11], [12].

There are various methods of generating fringe patterns. In recent years, digital projectors have been widely used to obtain fringe patterns [13]–[15]. The advantage of utilizing digital projectors for FPP is its simplicity and controllability. However, it is very difficult to obtain a pure sinusoidal fringe pattern by digital projectors due to the existence of geometrical distortion and color distortion. Meanwhile, we can note that for all the previously mentioned methods, it has been assumed that fringe patterns used for profilometry are pure sinusoidal or can be filtered to be sinusoidal by using digital filters to pick up the fundamental frequency component while eliminating the higher harmonics. However, in most practical cases, the filter cannot be ideal. Digital filtering can only suppress but not remove the harmonic components so that the results are still not purely sinusoidal. Moreover, when the deformed fringe pattern has an overlapped spectrum, bandpass filtering will be unavailable if a precise measurement is required. Therefore, errors will arise if the surface measurement is based on pure sinusoidal assumption. This problem motivates us to look for a new method to reconstruct the 3-D profile based on nonsinusoidal fringe patterns.

At the beginning of this paper, we take the FTP method as an example to make a quantitative analysis of the errors introduced by harmonics. The analytical result shows that the harmonic error is notable and cannot be ignored for profilometry. To reduce the errors, in Section III, we present a generalized model, which does not require the projected fringe pattern to be sinusoidal or periodic. Based on the derived mathematical model, Section IV proposes a shift estimation (SE) method to reconstruct 3-D surfaces from nonlinearly distorted fringe patterns. Because of the advantage of the generalized model, our algorithm depends neither on any particular structure of projected fringe patterns nor on the prior knowledge of the characteristics of projection systems. In Sections V and VI, the effectiveness of the proposed mathematical model and SE method has been confirmed by simulation and experimental results, which demonstrate that, compared with the conventional analysis model, the proposed model provides much improved precision, especially when the expected sinusoidal fringe patterns are distorted by unknown factors. Section VII concludes this paper.

Manuscript received March 22, 2007; revised September 19, 2007.

Y. Hu, J. Xi, and J. F. Chicharo are with the School of Electrical Computer and Telecommunications Engineering, University of Wollongong, Wollongong, NSW 2522, Australia (e-mail: jiangtao@uow.edu.au).

Z. Yang was with the Department of Electronic and Information Engineering, Huazhong University of Science and Technology, Wuhan 430074, China. He is now with Huazhong Normal University, Wuhan, 430079, China.

E. Li is with Tianjin University, Tianjin, 300072, China, and also with the School of Electrical Engineering and Telecommunications, University of New South Wales, Sydney, NSW 2052, Australia, and with the School of Engineering Physics, University of Wollongong, Wollongong, NSW 2522, Australia.

Digital Object Identifier 10.1109/TIM.2007.909417

II. Harmonic Error Analysis

A schematic diagram of a typical FPP system is shown in Fig. 1.

For simplicity, we consider a cross section of the object surface for a given y coordinate. Hence, the intensity of fringe patterns captured by the CCD camera and the height distribution function of the object surface can be expressed as a function with a single variable x. Meanwhile, if we consider the influence of the mth-order harmonic, after discarding the dc

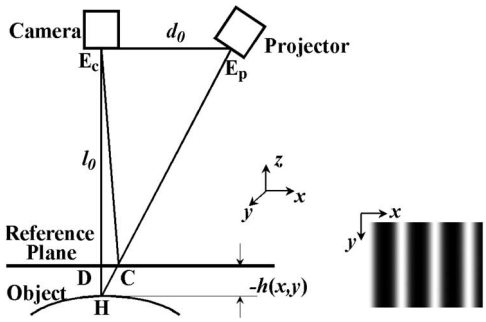

Fig. 1. Schematic diagram of the FPP system.

component, the fringe pattern projected on the reference plane can be expressed as

$$g(x) = b\cos(2\pi f_0 x) + c_m \cos(m \cdot 2\pi f_0 x) \tag{1}$$

where c_m denotes the amplitude of the mth-order harmonic. Meanwhile, deformed by the profile of the object, the fringe pattern on the object surface can be expressed as [3], [4]

$$\tilde{g}(x) = b\cos\left(2\pi f_0 x + \phi(x)\right) + c_m \cos\left(m \cdot (2\pi f_0 x + \phi(x))\right) \tag{2}$$

where $\phi(x)$ is the phase shift caused by the height distribution of the object. Accordingly, $G(x)$ and $\tilde{G}(x)$, which are the complex signals of $g(x)$ and $\tilde{g}(x)$, can be expressed as

$$G(x) = b \cdot \exp\left(i\xi(x)\right) + c_m \cdot \exp\left(i\left(m\xi(x)\right)\right) \tag{3}$$

where $\xi(x) = 2\pi f_0 x$, and

$$\begin{aligned}\tilde{G}(x) &= b \cdot e^{i(2\pi f_0 x + \phi(x))} + c_m \cdot e^{i(2\pi f_0 x + \phi(x))m} \\ &= b \cdot e^{i(\xi(x)+\phi(x))} + c_m \cdot e^{i(\xi(x)+\phi(x))m}.\end{aligned} \tag{4}$$

By the FTP method, we can obtain $\hat{\phi}$, which is the estimation of the phase map ϕ, by

$$\hat{\phi} = \mathrm{Im}\left(\log\left(\tilde{G}(x)G^*(x)\right)\right) \tag{5}$$

where $\log(\cdot)$ denotes a natural logarithm function, $\mathrm{Im}(\cdot)$ is the operation to get the imaginary part of a complex number, and G^* is the complex conjugate of G. Let $p_m = c_m^2/b^2$, which represents the power ratio of the mth-order harmonic to the fundamental component. Then, we have

$$\begin{aligned}\hat{\phi} &= \mathrm{Im}\left(\log\left(b \cdot e^{i(\xi+\phi)} + c_m \cdot e^{i(\xi+\phi)m}\right)\right. \\ &\qquad \left. + \log\left(b \cdot e^{-i\xi} + c_m \cdot e^{-i(m\xi)}\right)\right) \\ &= \mathrm{Im}\left(\log\left(e^{i(\xi+\phi)} + \sqrt{p_m} \cdot e^{i(\xi+\phi)m}\right)\right. \\ &\qquad \left. + \log\left(e^{-i\xi} + \sqrt{p_m} \cdot e^{-i(m\xi)}\right)\right) \\ &= \mathrm{Im}\left(i(\xi+\phi) + \log\left(1 + \sqrt{p_m} \cdot e^{i(\xi+\phi)(m-1)}\right)\right. \\ &\qquad \left. - i\xi + \log\left(1 + \sqrt{p_m} \cdot e^{-i\xi(m-1)}\right)\right) \\ &= \mathrm{Im}\left(i\phi + \log\left(1 + \sqrt{p_m} \cdot e^{i(\xi+\phi)(m-1)}\right)\right. \\ &\qquad \left. + \log\left(1 + \sqrt{p_m} \cdot e^{-i\xi(m-1)}\right)\right) \\ &= \phi + \mathrm{Im}\left(\log\left(1 + \sqrt{p_m} \cdot e^{i(\xi+\phi)(m-1)}\right)\right. \\ &\qquad \left. + \log\left(1 + \sqrt{p_m} \cdot e^{-i\xi(m-1)}\right)\right).\end{aligned} \tag{6}$$

Hence, the estimation error of the phase can be expressed as

$$\begin{aligned}\varepsilon &= \hat{\phi} - \phi \\ &= \mathrm{Im}\left(\log\left(1 + \sqrt{p_m} \cdot e^{i(\xi+\phi)(m-1)}\right)\right. \\ &\qquad \left. + \log\left(1 + \sqrt{p_m} \cdot e^{-i\xi(m-1)}\right)\right) \\ &= \mathrm{Im}\left(\log\left(1 + \sqrt{p_m} \cdot e^{i(\xi+\phi)(m-1)}\right)\right) \\ &\qquad + \mathrm{Im}\left(\log\left(1 + \sqrt{p_m} \cdot e^{-i\xi(m-1)}\right)\right).\end{aligned} \tag{7}$$

By considering the operation of $\mathrm{Im}(\log(\cdot))$, the phase angle of the complex number can be derived. We can define a function $\Lambda(\cdot)$ to represent this operation as follows:

$$\begin{aligned}\Lambda(\alpha) &= \mathrm{Im}\left(\log\left(1 + \sqrt{p_m} \cdot e^{i\alpha(m-1)}\right)\right) \\ &= \arctan\left(\frac{\sqrt{p_m}\sin\left(\alpha(m-1)\right)}{1 + \sqrt{p_m}\cos\left(\alpha(m-1)\right)}\right).\end{aligned} \tag{8}$$

Therefore, we have

$$\begin{aligned}\varepsilon &= \Lambda(\xi+\phi) + \Lambda(-\xi) \\ &= \Lambda(\xi+\phi) - \Lambda(\xi).\end{aligned} \tag{9}$$

Hence, the maximum error of the phase is

$$\varepsilon_{\max} = \Lambda_{\max}(\xi) - \Lambda_{\min}(\xi) \tag{10}$$

By letting $d\Lambda/d\xi = 0$, we can derive the maximum and minimum values of Λ, respectively, by

$$\Lambda_{\max} = \arctan\left(\sqrt{\frac{p_m}{1-p_m}}\right) \tag{11}$$

$$\Lambda_{\min} = -\arctan\left(\sqrt{\frac{p_m}{1-p_m}}\right). \tag{12}$$

Then, (10) can be expressed as

$$\varepsilon_{\max} = 2\arctan\left(\sqrt{\frac{p_m}{1-p_m}}\right). \tag{13}$$

For the conventional model, the height distribution is calculated by [3], [4], and [16]

$$h(x) = \frac{l_0\phi(x)}{\phi(x) - 2\pi f_0 d_0} \tag{14}$$

where l_0 and d_0 are the distance from the projector to the reference plane and to the CCD camera, respectively. An equivalent

form of (14) is

$$\phi(x) = \frac{2\pi f_0 d_0 h(x)}{h(x) - l_0} \tag{15}$$

and because the projector always locates far enough from the object, we have $l_0 \gg h(x)$. Therefore, $\phi(x)$ can be expressed approximately as

$$\phi(x) \approx \frac{2\pi f_0 d_0 h(x)}{-l_0} \tag{16}$$

then, we have

$$h(x) \approx -\frac{l_0}{2\pi f_0 d_0}\phi(x). \tag{17}$$

Hence, substituting (13) into this equation, the maximum absolute error of the height distribution can be expressed as

$$\beta = \frac{l_0}{\pi f_0 d_0} \cdot \arctan\left(\sqrt{\frac{p_m}{1-p_m}}\right). \tag{18}$$

For instance, if we assume that l_0 is 2 m and d_0 is 1 m, the maximum height of the object is 100 mm, and the spatial period of fringe pattern is 0.1 m, which implies that $f_0 = 10/\text{m}$. When $p = 0.01$, i.e., when the harmonic has only -20 dB of power compared with the fundamental component, the relative height error will reach 6.37%, which is not a negligible error for measurement. Therefore, when the projected fringes are distorted, we have to look for a new method to improve the precision.

III. Generalized Analysis Model

As shown in Fig. 1, we assume that l_0, which is the distance between the camera and the reference plane, is long enough so that the reflected light beams captured by CCD camera from the reference plane and the object are parallel. Meanwhile, because of the long distance, those parallel light beams reflected to the camera can be regarded as being vertical to the reference plane. Additionally, consistent with Section II, for simplicity, we only consider the cross sections of the object. Hence, the projected fringe patterns can be denoted by the functions with only one independent variable x for a given y coordinate, and the results can be extended to other values of y. We use $s(x)$ and $d(x)$ to represent the fringe pattern projected onto the reference plane and onto the object surface, respectively. Similarly, the height distribution function is denoted by $h(x)$.

To establish the relationship between $s(x)$ and $d(x)$, we consider a beam of light that corresponds to a pixel of the fringe pattern, denoted as E_pCH in Fig. 1. It is seen that the light beam is projected at point C and reflected back to the camera if the reference plane exists. When the reference plane is removed, the same beam will be projected onto point H on the surface of the object, which is reflected to the camera via point D. This implies that the x coordinate of point H in the image of the object surface is equal to the x coordinate of point D in the image of the reference plane, because points D and H are on the same reflected beam from point H to the camera. Assuming that the object surface and the reference plane have the same reflective characteristics, $s(x)$ at location C should exhibit the same intensity as $d(x)$ does at location D because they originate from the same point of the fringe pattern created by the projector. Hence, we have

$$d(x_d) = s(x_c). \tag{19}$$

We use u to denote the distance from C to D, i.e.,

$$u = x_d - x_c \tag{20}$$

where x_c and x_d are the coordinate locations of points C and D, respectively. From (19) and (20), we have

$$d(x_d) = s(x_d - u). \tag{21}$$

Obviously, u varies with the height of point H on the object surface.

Meanwhile, because triangles E_pHE_c and CHD are similar, we have

$$\frac{x_c - x_d}{-h(x_h)} = \frac{d_0}{l_0 - h(x_h)} \tag{22}$$

where x_h is the x coordinate of point H, l_0 is the distance between the camera and the reference plane, and d_0 is the distance between the camera and the projector.

As mentioned above, point H has the same x coordinate as point D does in captured images, which implies that $x_h = x_d$. Therefore, (22) can be rewritten as

$$\frac{x_c - x_d}{-h(x_d)} = \frac{d_0}{l_0 - h(x_d)}. \tag{23}$$

As defined in (20), (23) can be expressed as

$$\frac{-u}{-h(x_d)} = \frac{d_0}{l_0 - h(x_d)}. \tag{24}$$

As the height distribution $h(x)$ is a function of x_d, u should also be a function of x_d. Then, we have

$$u(x_d) = \frac{d_0 h(x_d)}{l_0 - h(x_d)}. \tag{25}$$

An equivalent representation is

$$h(x_d) = \frac{l_0 u(x_d)}{d_0 + u(x_d)}. \tag{26}$$

Therefore, (21) can be expressed as

$$d(x_d) = s\left(x_d - u(x_d)\right) \tag{27}$$

where $u(x_d)$ is given by (25).

To simplify (27) and considering the model only mathematically, we let $x_d = x$. Then, we can derive a general mathematical model from (26) and (27) as follows:

$$d(x) = s\left(x - u(x)\right) \tag{28}$$

$$h(x) = \frac{l_0 u(x)}{d_0 + u(x)} \tag{29}$$

Equations (28) and (29) reveal that the deformed signal $d(x)$ is a shifted version of $s(x)$, and the shift function $u(x)$ varies with the height of the object. This implies that the shift signal $u(x)$ contains all the 3-D information of the object surface. By using (28) and (29), as long as we can obtain the function $u(x)$, the surface reconstruction can be achieved.

Equation (28) expresses the general relationship between the deformed signal and the projected signal. Note that the projected signal $s(x)$ can be of any form, and hence, it is not necessarily required to be sinusoidal. Therefore, compared with the traditional model, (28) and (29) can be regarded as a generalized analysis model for FPP, and the conventional analysis model is only a special case of the generalized model proposed earlier. They would have a consistent form when cosinusoidal fringe patterns are projected onto object surfaces. As a matter of fact, by letting $s(x)$ be a cosinusoidal signal, we can simply derive the traditional analysis model from our proposed generalized model. If we use sinusoidal or cosinusoidal fringe patterns, the projected signal can be expressed as

$$s(x) = A + B\cos(2\pi f_0 x) \tag{30}$$

where A is the background illumination that can be regarded as a constant, and B is the amplitude of intensity of cosinusoidal fringe patterns. By substituting (30) into (28), the deformed signal is

$$\begin{aligned} d(x) &= s\left(x - u(x)\right) \\ &= A + B\cos\left(2\pi f_0\left(x - u(x)\right)\right) \\ &= A + B\cos\left(2\pi f_0 x - 2\pi f_0 u(x)\right) \\ &= A + B\cos\left(2\pi f_0 x + \phi(x)\right) \end{aligned} \tag{31}$$

where

$$\phi(x) = -2\pi f_0 u(x). \tag{32}$$

As expected, for the case where a cosinusoidal fringe pattern is used, the deformed signal $d(x)$ is a phase-modulated signal. Hence, all of the conventional analysis methods initially attempt to demodulate the deformed signals and retrieve the phase map $\phi(x)$. Then, by using the relationship between the phase shift function $\phi(x)$ and the height distribution $h(x)$, the shapes of objects can be reconstructed. When a sinusoidal fringe pattern is used, we can easily derive the relationship between $\phi(x)$ and $h(x)$ by our proposed generalized model. Note that, in (32), an equivalent form is

$$u(x) = -\frac{\phi(x)}{2\pi f_0}. \tag{33}$$

By substituting (33) into (29), we can derive the well-known equation

$$h(x) = \frac{l_0\phi(x)}{\phi(x) - 2\pi f_0 d_0} \tag{34}$$

which is just (14). As a classical formula, it appears in most of the articles on FPP (e.g., [3], [4], and [16]).

As mentioned earlier, essentially, the conventional model is simply a particular case of our proposed model when the projected signal on the reference plane $s(x)$ is exactly sinusoidal. However, in practical cases, especially when we are using a digital projector to generate fringe patterns, it is very difficult to obtain a pure sinusoidal signal. Fortunately, our proposed generalized model does not require the projected signal to be sinusoidal. This implies that, although the projected signal has been distorted by some unknown factors, accurate profilometry is still practicable, as long as we can find out a method to retrieve the shift signal $u(x)$ from the captured signals $s(x)$ and $d(x)$. Based on our proposed generalized model, we present an SE method to retrieve the shift function $u(x)$ in Section IV.

IV. SE Method

According to the generalized model presented in Section III, the value of the shift function $u(x)$ determines the height distribution $h(x)$ so that the height distribution of the object surface can be obtained if we have $u(x)$. Hence, we should track the values of the shift function $u(x)$ for each point x by using $s(x)$ and $d(x)$. For this purpose, we use a square error, which is defined as follows, as an objective function with respect to $\hat{u}(x)$ that denotes the estimation of the value of $u(x)$ at point x:

$$e^2\left(\hat{u}(x)\right) = \left[d(x) - s\left(x - \hat{u}(x)\right)\right]^2. \tag{35}$$

To minimize e^2, we use a gradient-based method in obtaining $\hat{u}(x)$ in an iterative way, i.e.,

$$\hat{u}_{m+1} = \hat{u}_m - \eta \left.\frac{de^2}{d\hat{u}}\right|_{\hat{u}=\hat{u}_m} \tag{36}$$

where η is the learning rate. The gradient can be derived as

$$\begin{aligned} \left.\frac{de^2}{d\hat{u}}\right|_{\hat{u}=\hat{u}_m} &= 2e\left.\frac{de}{d\hat{u}}\right|_{\hat{u}=\hat{u}_m} \\ &= -2e\left.\frac{ds}{d\hat{u}}\right|_{\hat{u}=\hat{u}_m} \\ &= -2e\frac{s\left(x - (\hat{u}_m + 1)\right)s\left(x - (\hat{u}_m - 1)\right)}{(\hat{u}_m + 1) - (\hat{u}_m - 1)} \\ &= -e\left[s(x - \hat{u}_m - 1) - s(x - \hat{u}_m + 1)\right] \\ &= -\left[d(x) - s(x - \hat{u}_m)\right] \\ &\quad \times \left[s(x - \hat{u}_m - 1) - s(x - \hat{u}_m + 1)\right]. \end{aligned} \tag{37}$$

By substituting (37) into (36), we can have the following iterative equation for calculating the estimation of the value of the shift function $u(x)$ at each point x:

$$\begin{aligned} \hat{u}_{m+1}(x) = \hat{u}_m(x) &+ \eta\left[d(x) - s\left(x - \hat{u}_m(x)\right)\right] \\ &\times \left[s\left(x - \hat{u}_m(x) - 1\right) - s\left(x - \hat{u}_m(x) + 1\right)\right]. \end{aligned} \tag{38}$$

For each point x, the iteration continues until convergence. In other words, if $|\hat{u}_{m+1} - \hat{u}_m|$ is less than a given lower bound, we can obtain an estimation of the value of $u(x)$ at point x by $\hat{u}(x) = \hat{u}_m(x)$. Considering the continuity of the

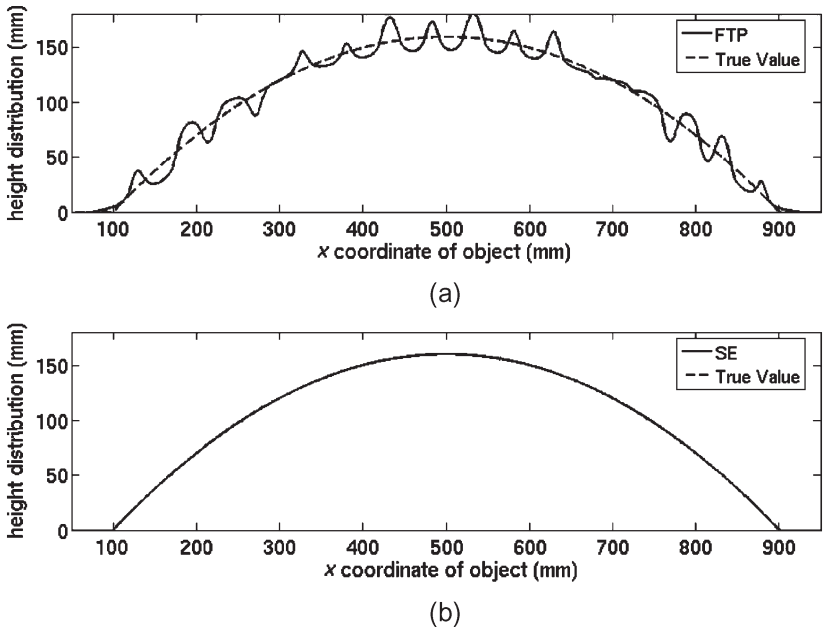

Fig. 2. Reconstruction results and error comparison.

profiles, we can use the converged value $\hat{u}(x)$ as the initial value for the next point $x+1$, i.e., let $\hat{u}_1(x+1) = \hat{u}(x)$, and then, continue doing the iteration for the next point $x+1$ so that faster convergence can be achieved.

V. Simulation

Simulations have been performed to verify the correctness of the generalized model and the effectiveness of our proposed SE method. In our simulation, we use a paraboloid object surface whose maximum height is 160 mm and the projected fringe pattern is generated from a cosinusoidal signal distorted by a nonlinear function given by

$$S\left(g(x)\right) = 0.00156g^2(x) + g(x) + C \tag{39}$$

where C is a constant that can be ignored, as it does not affect the reconstruction results, and $g(x) = A\cos(2\pi f_0 x)$, where f_0 is the spatial frequency of the fringe pattern, which is assumed to be 0.01/mm in our simulation, i.e., the spatial period of the fringe pattern is assumed to be 100 mm. Assuming that 8-bit quantification is used for the CCD camera, then, A, which is the amplitude of the cosinusoidal signal $g(x)$ is assumed to be 128. Meanwhile, we assume that l_0 and d_0 in Fig. 1 are equal to 5 and 2 m, respectively. The spatial resolution of the captured image is assumed to be 1 pixel/mm.

Substituting $g(x) = A\cos(2\pi f_0 x)$ into (39) and discarding the dc component, we have

$$s(x) = 128\cos(2\pi f_0 x) + 12.8\cos\left(2\pi\cdot(2f_0)x\right). \tag{40}$$

Note that, for the projected fringe pattern given by (40), the second-order harmonic only has -20 dB of power compared with the fundamental component. Corresponding to (40), the deformed fringe pattern can be expressed as [3], [4]

$$d(x) = 128\cos\left(2\pi f_0 x + \phi(x)\right) + 12.8\cos\left(2\pi\cdot(2f_0)x + 2\phi(x)\right) \tag{41}$$

where $\phi(x)$ is the phase shift caused by the object surface. It has been well known that, with the conventional model, after demodulating $\phi(x)$, the surface height distribution can be calculated by the relationship between $\phi(x)$ and the height distribution $h(x)$, which is expressed as (14).

Using the fringe pattern given by (40) and (41), we can reconstruct the object surface by the conventional FTP method and the SE method, respectively. The comparative results are shown in Fig. 2.

In Fig. 2(a), the solid line is the measurement result by the FTP method, whereas the dashed line refers to the object surface, which is the true value of the height distribution. This figure shows that nonlinear distortion introduces noticeable errors when the FTP method is used, although the nonlinear distortion is so slight that the coefficient of the square item in (39) is only 0.00156 and the second-order harmonic only has -20 dB of power compared with the fundamental component. Moreover, the reconstructed surface by using the FTP method is jagged and rough.

Comparatively, by our proposed model and the SE method, we can obtain a much better reconstruction result shown in Fig. 2(b). As in Fig. 2(a), the dashed line is the true value, and the solid line represents the reconstruction result by using our proposed generalized model and the SE method. It can be seen that the reconstruction result by the SE method is almost identical to the true values. The measurement accuracy is significantly improved, and the reconstructed surface is much smoother than using the FTP method.

Fig. 3 shows the absolute errors of the reconstructed height distribution.

The solid and dashed lines represent the reconstruction error by using the FTP and SE methods, respectively. We can see that measurement accuracy is significantly improved by the generalized model and the SE method.

Further, we did another simulation for a more complex surface to show the performance of the proposed method. The

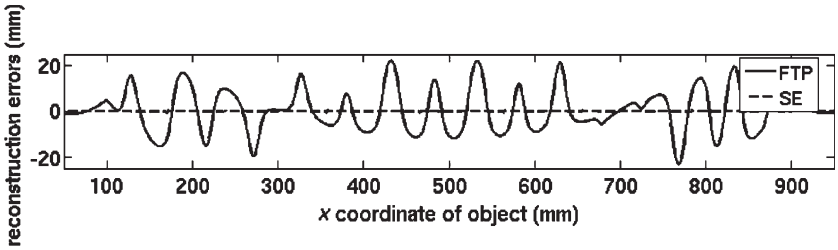

Fig. 3. Absolute reconstruction errors.

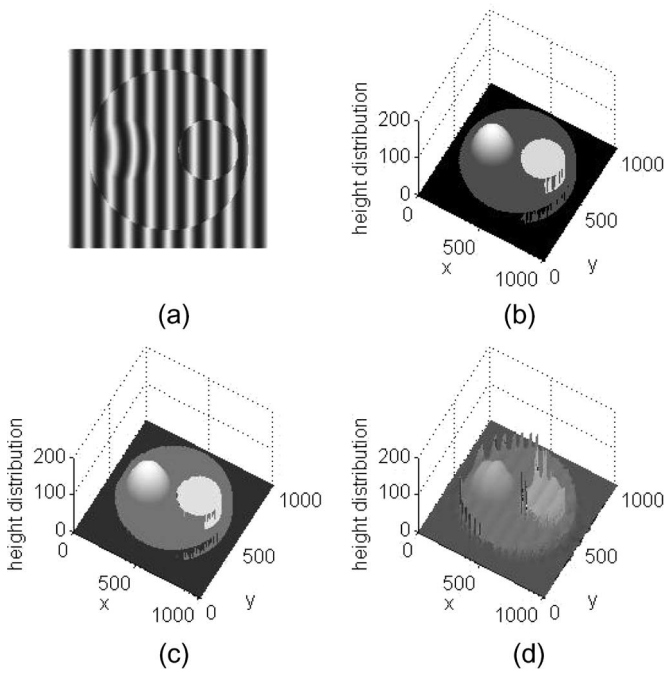

Fig. 4. Simulation results for measuring a more complex surface. (a) Fringe pattern on the object surface. (b) Object surface for simulation. (c) Reconstruction result by using SE. (d) Reconstruction result by using FTP.

surface designed for the simulation is shown in Fig. 4(b), and Fig. 4(a) demonstrates the fringe pattern image captured on the object surface.

Fig. 4(c) and (d) shows the reconstruction results by using the proposed SE and FTP algorithms, respectively, which also shows that the object surface reconstructed by SE is very smooth and is almost identical to the theoretical values, but the surface reconstructed by using FTP is very rough and is significantly influenced by nonlinear distortions.

To compare the performance for different algorithms more clearly, cross sections of the reconstructed surfaces are shown in Fig. 5, where solid and dashed lines represent the reconstruction results by using SE and FTP, respectively. The dotted line is the theoretical value of the height distribution.

It can be seen that the reconstruction result by using SE is very accurate, even for a complex object with sharp edges.

VI. Experimental Results

In our experiment, an InFocus LP530 DLP is used to generate sinusoidal fringe patterns, and we employ a DuncanTech

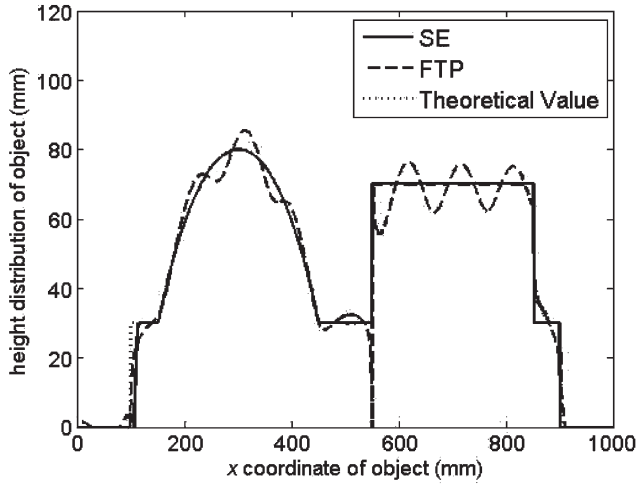

Fig. 5. Cross section of simulation results for measuring a more complex surface.

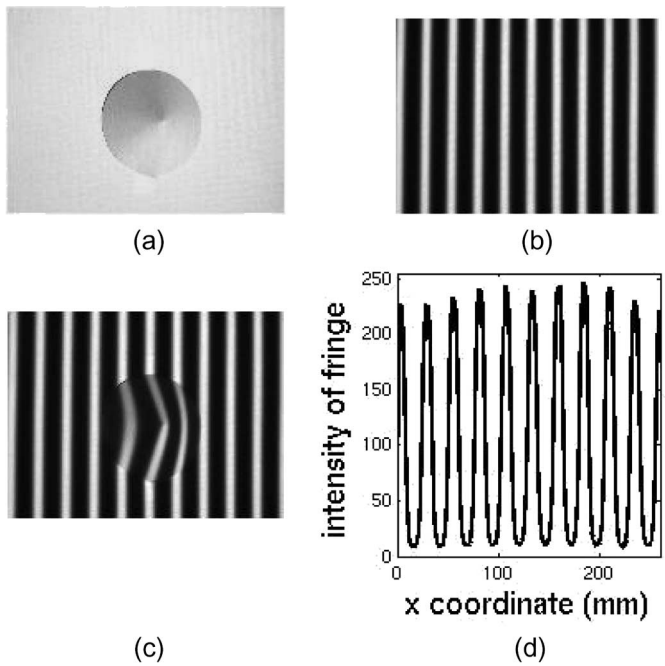

Fig. 6. Projected fringes and the measured cone.

MS3100-RGB 3CCD to capture the images. The parameters d_0 and l_0 are 200 and 81 cm, respectively. The equivalent spatial period of the fringe pattern is 25.7 mm. The object that we try to measure is a cone that is 38 mm high, and the diameter of its bottom surface is 94 mm, which is shown in Fig. 6(a).

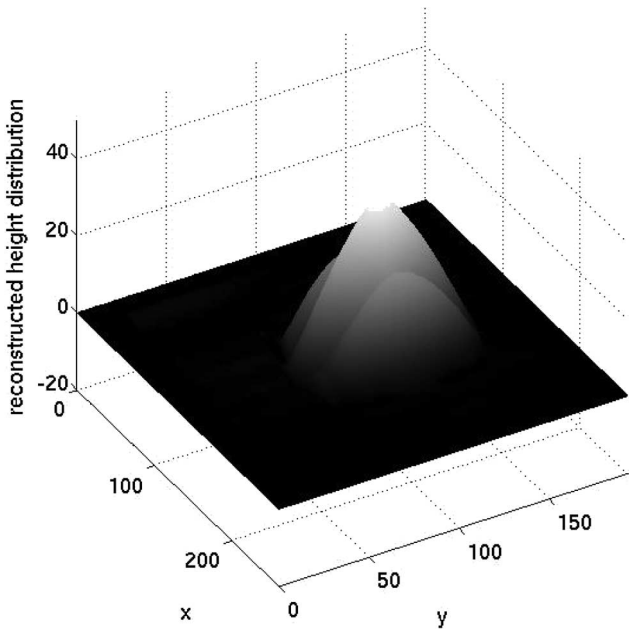

Fig. 7. Experimental result by FTP.

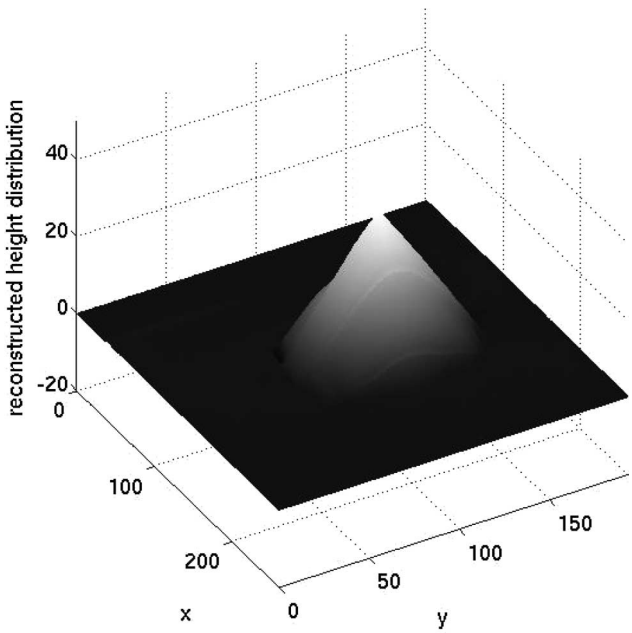

Fig. 8. Experimental result by SE.

The fringe pattern projected onto the reference plane and on the object surface are shown in Fig. 6(b) and (c). Fig. 6(d) is a cross section of Fig. 6(d). As shown in Fig. 6(d), the fringe pattern projected onto the reference plane does not appear to be purely sinusoidal. By using this captured signal, the reconstruction results by FTP is shown in Fig. 7.

We can see that due to the nonlinear distortion, the reconstructed surface by FTP is jagged. The average error to measure the object by using FTP is 7.142 mm. In contrast, the error by using the SE method is 1.024 mm. As demonstrated in Fig. 8, the profile measured by our proposed model and algorithm is much smoother than the reconstruction result of FTP.

By our experiment, the significant improvement of our proposed method is clearly demonstrated. We should say that the enhancement of performance is due to the fact that the generalized model can more exactly describe the relationship between the projected signals on the reference plane and on the object when the nonlinear distortion exists.

VII. Conclusion

In this paper, we have presented a generalized model for FPP, which describes a general relationship between the projected signal and the deformed signal. Based on the generalized model, we present an SE method to implement profilometry. With the generalized model and the SE method, the constraint of using sinusoidal signals has been completely removed. In other words, even if the original signal is nonlinearly distorted, we can still obtain an accurate reconstruction result without any prior knowledge of the characteristics of the profilometry system. The correctness of the generalized model and effectiveness of the SE method have been completely confirmed by our simulation and experimental results.

References

[1] M. Takeda and K. Mutoh, "Fourier transform profilometry for the automatic measurement of 3-D object shapes," *Appl. Opt.*, vol. 22, no. 24, pp. 3977–3982, Dec. 1983.

[2] M. Takeda, H. Ina, and S. Kobayashi, "Fourier-transform method of fringe-pattern analysis for computer-based topography and interferometry," *J. Opt. Soc. Amer.*, vol. 72, no. 1, pp. 156–160, Jan. 1982.

[3] X. Su and W. Chen, "Fourier transform profilometry: A review," *Opt. Lasers Eng.*, vol. 35, no. 5, pp. 263–284, May 2001.

[4] X. Su, W. Chen, Q. Zhang, and Y. Chao, "Dynamic 3-D shape measurement method based on FTP," *Opt. Lasers Eng.*, vol. 36, no. 1, pp. 49–64, Jul. 2001.

[5] J. Pearson, F. Lilley, D. Burton, J. Atkinson, S. Kshirsagar, D. Search, and C. Hobson, "Phase-measuring methods for the measurement of three-dimensional shape in automated inspection of manufactured electronic assemblies," in *Proc. SPIE—Machine Vision Applications Industrial Inspection II*, 1994, vol. 2183, pp. 238–248.

[6] V. Srinivasan, H. Liu, and M. Halioua, "Automated phase-measuring profilometry of 3-D diffuse objects," *Appl. Opt.*, vol. 23, no. 18, pp. 3105–3108, 1984.

[7] X. Su, W. Zhou, G. von Bally, and D. Vukicevic, "Automated phase-measuring profilometry using defocused projection of Ronchi grating," *Opt. Commun.*, vol. 94, no. 6, pp. 561–573, Dec. 1992.

[8] H. Su, J. Li, and X. Su, "Phase algorithm without the influence of carrier frequency," *Opt. Eng.*, vol. 36, no. 6, pp. 1799–1805, 1997.

[9] S. Toyooka and Y. Iwaasa, "Automatic profilometry of 3-D diffuse objects by spatial phase detection," *Appl. Opt.*, vol. 25, no. 10, pp. 1630–1633, May 1986.

[10] R. Rodriguez-Vera and M. Servin, "Phase locked loop profilometry," *Opt. Laser Technol.*, vol. 26, no. 6, pp. 393–398, 1994.

[11] A. Moore and F. Mendoza-Santoyo, "Phase demodulation in the space domain without a fringe carrier," *Opt. Lasers Eng.*, vol. 23, no. 5, pp. 319–330, 1995.

[12] J. Villa, M. Servin, and L. Castillo, "Profilometry for the measurement of 3-D object shapes based on regularized filters," *Opt. Commun.*, vol. 161, no. 1, pp. 13–18, Mar. 1999.

[13] L. Kinell, "Multichannel method for absolute shape measurement using projected fringes," *Opt. Lasers Eng.*, vol. 41, no. 1, pp. 57–71, Jan. 2004.

[14] P. Huang, Q. Ho, F. Jin, and F. Chiang, "Color-enhanced digital fringe projection technique for high-speed three-dimensional surface contouring," *Opt. Eng.*, vol. 38, no. 6, pp. 1065–1071, Jun. 1999.

[15] Y. Hu, J. Xi, E. Li, J. Chicharo, Z. Yang, and Y. Yu, "A calibration approach for decoupling colour cross-talk using nonlinear blind signal separation network," in *Proc. IEEE Conf. Optoelectron. Microelectron. Mater. Devices*, 2004, pp. 265–268.

[16] F. Berryman, P. Pynsent, and J. Cubillo, "A theoretical comparison of three fringe analysis method for determining the three dimensional shape of an object in the presence of noise," *Opt. Lasers Eng.*, vol. 39, no. 1, pp. 35–50, Jan. 2003.

Yingsong Hu received the B.E. degree in telecommunications engineering from Huazhong University of Science and Technology, Wuhan, China, in 2000 and the Ph.D. degree in communication and information system in 2006.

He has been with the School of Electrical Computer and Telecommunications Engineering, University of Wollongong, Wollongong, Australia, since 2003 as a Visiting Fellow. His research interests are signal processing, image processing, telecommunication signal processing, and their applications.

Jiangtao Xi (M'95–SM'06) received the B.E. degree from Beijing Institute of Technology, Beijing, China, in 1982, the M.E. degree from Tsinghua University, Beijing, in 1985, and the Ph.D. degree from the University of Wollongong, Wollongong, Australia, in 1996, all in electrical engineering.

He was a Postdoctoral Fellow with the Communications Research Laboratory, McMaster University, ON, Canada, from 1995 to 1996 and a Member of Technical Staff at Bell Laboratories, Lucent Technologies Inc., NJ, from 1996 to 1998. From 2000 to 2002, he was with the TCL IT Group Company, China, as its Chief Technical Officer. In 2003, he rejoined the University of Wollongong as a Senior Lecturer, where he is currently an Associate Professor with the School of Electrical Computer and Telecommunications Engineering. His research interests are signal processing and its applications in various areas, including photonics, optical electronics, and telecommunications.

Zongkai Yang (SM'06) received the B.E. and M.E. degrees from Huazhong University of Science and Technology (HUST), Wuhan, China, in 1985 and 1988, respectively, and the Ph.D. degree from Xi'an Jiaotong University, Xi'an, China, in 1991.

From 1991 to 1993, he was with the School of Electronic and Information Engineering, HUST, working on his postdoctoral research. From 1994 to 1995, he was with Korea University, Seoul, Korea, working on his doctoral research. In 1993, he joined the School of Electronic and Information Engineering, HUST, as the Director of the Electronic Business Center and the Deputy Dean of the Electronic and Information Department. From 1994 to 2003, he was a Visiting Researcher and a Senior Visiting Scholar at Korea University, Silicon Valley in the U.S., University of Wollongong, Wollongong, Australia, Nanyang Technological University, Singapore, and the University of Michigan, Ann Arbor. He is currently with Huazhong Normal University, Wuhan, as the Vice President. He is the author of more than 80 journal and conference papers. His research interests are signal processing, network communication, and information technology.

Enbang Li received the B.Sc., M.Sc., and Ph.D. degrees from Tianjin University, Tianjin, China, in 1984, 1987, and 1990, respectively.

He was with the University of Wollongong, Wollongong, Australia, and JDS Uniphase, Sydney, Australia, for more than ten years. He is currently a Professor of optoelectronics with Tianjin University, a Professorial Visiting Fellow with the School of Electrical Engineering and Telecommunications, University of New South Wales, Sydney, Australia, and a Visiting Principal Fellow with the School of Engineering Physics, University of Wollongong. His research interests include laser diagnostics, fiber Bragg grating devices and techniques for fiber communications and fiber sensing applications, fiber lasers, and photonic crystals. He is the author or coauthor of more than 100 technical publications.

Joe F. Chicharo (M'89–SM'94) received the B.Sc. (with first-class honors) and Ph.D. degrees in electrical engineering from the University of Wollongong, Wollongong, Australia, in 1983 and 1990, respectively.

Since 1985, he has been with the same university as a Lecturer (1985–1990), Senior Lecturer (1990–1993), Associate Professor (1994–1997), and Professor (since 1997). He is currently the Dean of the Faculty of Informatics, School of Electrical Computer and Telecommunications Engineering, University of Wollongong. From 2000 to 2003, he was the Research Director of the Australian Collaborative Research Center on Smart Internet Technology. He is the author of over 200 research publications. His research interests are signal processing, telecommunications, and information technology.